JOURNAL OF PROPULSION AND POWER
Vol. 22, No. 3, May–June 2006

Downstream Ramjet-Mode Combustion in a Dual-Mode Scramjet Engine

Kanenori Kato,* Takeshi Kanda,† Kan Kobayashi,‡ Kenji Kudo§, and Atsuo Murakami§
Japan Aerospace Exploration Agency, Miyagi 981-1525, Japan

Downstream combustion ramjet-mode operation in a dual-mode engine combustor was studied experimentally with a Mach 2.5 wind tunnel. In this downstream combustion ramjet mode, subsonic combustion was attained in the downstream straight-duct section without a geometrical throat. The experimental results are presented. The total temperature and the total pressure in the vitiation air heater were 800 K and 1.0 MPa, respectively. Pitot pressure and gas sampling were measured on the exit plane of the combustion model. The combustion conditions of the downstream combustion ramjet mode were compared with those of the usual upstream combustion ramjet mode. Better thrust performance and combustion were observed in the upstream combustion ramjet mode. However, in the case of the downstream combustion ramjet mode, injection of a larger amount of fuel was possible and a large impulse function was attained. The downstream straight duct was required for sufficient reaction. The fuel did not go far upstream in the separation region in pseudo-shock.

Nomenclature

ER = equivalence ratio
M = Mach number
P_i = wall pressure at the entrance of the combustor
P_p = pitot pressure
P_w = wall pressure
x = distance from backward-facing step
y = vertical distance from the bottom
z = transverse distance from side wall surface
η_c = combustion efficiency
ϕ = equivalence ratio

I. Introduction

VARIOUS air-breathing engines are being studied for space transportation systems. Each engine has a specific operation range. To decrease the weight of the propulsion system, an engine that operates in multiple operation modes is needed. To realize such an engine, ramjet-mode operation in a dual-mode engine has been studied.[1–4] Generally, in the ramjet-mode operation of dual-mode engine combustors, supersonic air flowing into the combustor is decelerated in the straight duct section of the isolator. Then the subsonic combustion gas is choked at the exit of the straight section of the combustor and accelerated in the divergent section. In the present study, we investigated a downstream combustion ramjet mode. Subsonic combustion was attained in the straight-duct section downstream of the divergent section without a geometrical throat.[3] The advantage of the downstream combustion ramjet mode is that the maximum wall pressure is less than that of the upstream combustion ramjet mode. Also, the maximum wall pressure appeared in the divergent duct and was available to generate thrust. Furthermore, this downstream combustion avoids inlet–combustor interaction. Application of this study to combined-cycle engines is now under consideration.[5]

In the present paper, the experimental results of two types of ramjet-mode operation are presented. A straight duct was installed in the combustor model downstream of the divergent section, and the condition of no duct was also tested for further reduction of the engine weight. Probing was conducted on the exit plane of the combustor model, pitot pressure was measured, and gas sampling was done. We compared the combustion conditions in the downstream combustion ramjet mode with those in the usual upstream combustion ramjet mode.

II. Experimental Facility

Figure 1 shows a schematic illustration of the test facility and the combustor model. The dual-mode engine combustor model was directly connected to a Mach 2.5 blowdown-type wind tunnel. The airflow was heated in a hydrogen vitiation heater. The cross section of the combustor entrance was 32 mm wide and 147.3 mm high. Air flowed into a constant cross-sectional area isolator, followed by a constant cross-sectional area combustor with a length of 96 mm. The isolator is used for isolation of the inlet from the influence of downstream combustion. There was a backward-facing step with a height of 3.2 mm at the end of the isolator for flame holding in the upstream combustion ramjet mode. The cross section of the combustor was 38.4×147.3 mm. There was a divergent-duct part downstream of the constant-duct part. The angle of the divergent section was 3.4 deg. The cross section of the divergent duct section was 67.2×147.3 mm at the exit. In this study, a straight-duct part with a length of 120 mm was attached downstream of the divergent-duct part. The y-axis indicates the distance from the bottom wall surface and the z-axis indicates the transverse distance from the side wall surface.

The combustor model had several fuel injection positions. In the upstream combustion ramjet mode, the position of fuel injection was at $x = 12.8$ mm at inj 1. In the case of the downstream combustion ramjet mode, the position of fuel injection was at $x = 432.8$ mm at inj 6. At each position, there were five fuel injection holes on a sidewall and four on the opposite sidewall. There were nine holes at each injection position in total. The pitch between the holes was 32 mm. The diameter of each injection hole was 4 mm, except for that of two holes. The diameter of those two was 2.8 mm. This was for the sake of uniformity of injected fuel concentration.

Presented as Paper 2005-617 at the AIAA 43rd Aerospace Sciences Meeting and Exhibit, Reno, NV, 10–13 January 2005; received 6 May 2005; revision received 22 September 2005; accepted for publication 4 October 2005.

*Senior Researcher, Combined Propulsion Research Group, Space Propulsion Center, 1 Koganezawa, Kimigaya, Kakuda. Member AIAA.
†Leader, Engine System Sub-group, Combined Propulsion Research Group, Space Propulsion Center, 1 Koganezawa, Kimigaya, Kakuda. Senior Member AIAA.
‡Researcher, Combustion and Control Sub-group, Combined Propulsion Research Group, Space Propulsion Center, 1 Koganezawa, Kimigaya, Kakuda. Member AIAA.
§Senior Researcher, Combined Propulsion Research Group, Space Propulsion Center, 1 Koganezawa, Kimigaya, Kakuda.

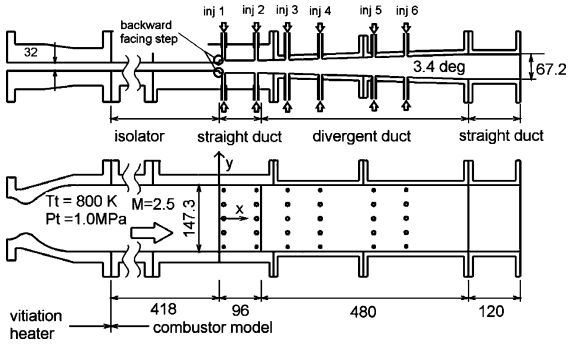

Fig. 1 Schematic illustration of the wind tunnel and combustor model.

The total pressure of the air used in this combustor model was 1.0 MPa. The nominal total temperature of the air was 800 K. This is in a typical enthalpy range of air under ramjet operation. Since the total temperature of the airflow was lower than the autoignition limit, a torch igniter[6] was installed on both walls. The position of each torch igniter was at $x = 392.8$ mm.

Pressure taps were installed on the centerline of the side wall. The measurement uncertainty was ± 0.1 kPa. The measured pressure was normalized by the wall pressure at the entrance of the combustor. Gas sampling was also conducted through these pressure taps to investigate the spread of fuel in the separation region. Sampled gas was analyzed by gas chromatography (Micro-GC CP2000®). The pitot rake installed at the exit of the downstream straight duct was water-cooled. Gas sampling was also conducted using this pitot rake.[7] The pitot pressure measurements were performed at 50 locations.

Another pitot rake was inserted into the divergent duct to investigate the velocity distribution in the separation region, which was uncooled. Pitot pressure measurement requires a very short period. However, because gas sampling needs a few seconds, it was not conducted.

III. One-Dimensional Calculation

To investigate the flow field in the combustor, one-dimensional calculation was conducted. The measured wall pressures were input data. The distributions of the combustion efficiency and the Mach number were outputs. The features and the procedures of the calculation model are as bellows:

1) Mass, energy, and impulse function were conserved.

2) Fuel was distributed only downstream of the injector.

3) Separation was assumed to be upstream of the fuel injector and no velocity in the separation region was assumed.

4) Downstream of the fuel injection, no separation was assumed.

5) Downstream of the fuel injection, the conservations were satisfied by changing the combustion efficiency.

The air and the combustion gas were in chemical equilibrium. Combustion gas was at the same static temperature and velocity as those of the residual fuel and the residual air. In the region of the pseudo-shock, flow is separated from the wall, and there is little or negative friction force on the wall surface.[8–11]

IV. Results and Discussion

A. Wall Pressure Distribution

Figure 2 shows the typical wall-pressure distributions of the upstream combustion ramjet mode and the downstream combustion ramjet mode. The fuel injection positions are shown in the figure by bars. In the case of the upstream combustion ramjet mode, the fuel was injected from position 1. In the case of the downstream combustion ramjet mode, the fuel was injected from position 6. The equivalence ratios were 0.3 for both cases. The torch position is also shown in the figure by TI. In each case, the torch position was in the divergent duct. In the case of the upstream combustion ramjet mode, the torch ignites in that position. The distribution of the no-fuel case is also plotted for comparison. The bars with "P" in the figure indicate the measurement position of the pitot pressure in the divergent duct.

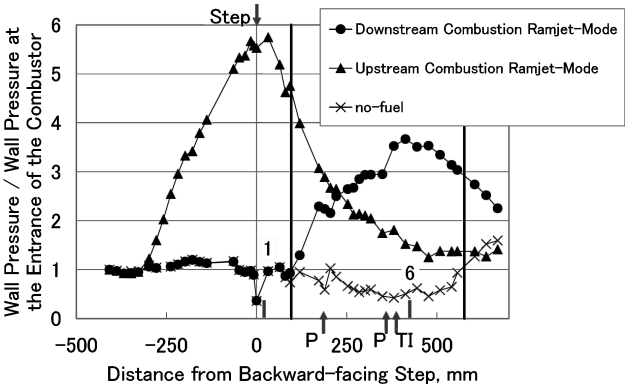

Fig. 2 Wall-pressure distributions for upstream combustion ramjet mode and downstream combustion ramjet mode with $\phi = 0.3$.

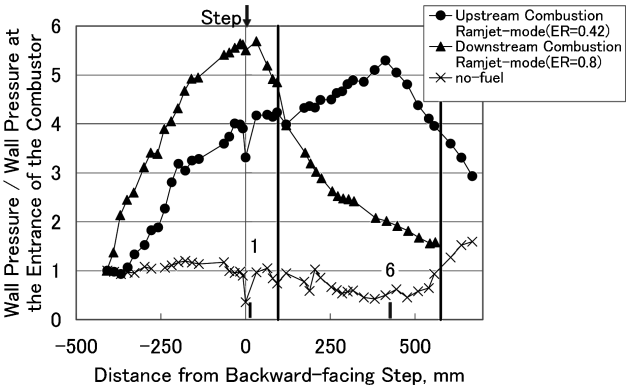

Fig. 3 Wall-pressure distributions for downstream combustion ramjet mode with maximum equivalence ratios do not influence the facility nozzle.

In the case of the upstream combustion ramjet mode, the maximum wall pressure appeared at the fuel injector in the constant-area duct and decreased in the divergent duct. The rise of P_w influenced the distribution of wall pressure in the isolator.

In the case of the downstream combustion ramjet mode, the maximum wall pressure appeared at the fuel injector in the divergent duct and there was no influence on the wall pressure upstream of the step. The maximum wall pressure was smaller than that of the upstream combustion ramjet mode. The pressure decreased toward the exit of the downstream straight duct. However, the pressure at the exit was higher than the atmospheric pressure. The combustion gas choked at the exit of the duct.

Figure 3 shows the wall-pressure distributions of the upstream combustion ramjet mode and the downstream combustion ramjet mode, which were of higher equivalence ratio mode not to influence the facility nozzle. In the case of high equivalence ratio, there was an influence on the wall pressure upstream of the step even in the downstream combustion ramjet mode. However, in the case of the downstream combustion ramjet mode with $\phi = 0.8$, there was no influence on the facility nozzle. In the case of the upstream combustion ramjet mode, the highest equivalence ratio that did not influence the facility nozzle was 0.45 (Ref. 4). However, in the case of the downstream combustion ramjet mode, the highest equivalence ratio that did not influence the facility nozzle was 0.86. It was possible to inject a larger amount of fuel in the case of the downstream combustion ramjet mode.

B. One-Dimensional Calculation

To examine the combustion conditions, one-dimensional calculation was conducted. Figures 4a and 4b show the estimated combustion efficiency and the averaged Mach number.

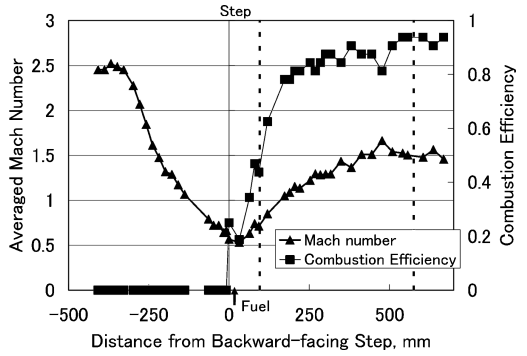

a) Upstream combustion ramjet mode

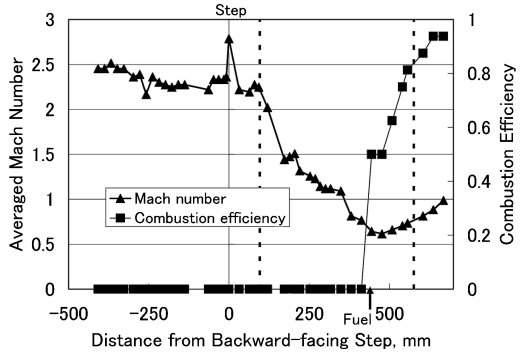

b) Downstream combustion ramjet mode

Fig. 4 Distributions of Mach number and combustion efficiency with equivalence ratio = 0.3.

In upstream combustion ramjet mode, the estimated Mach number decreased to below unity in the isolator section and the constant cross-sectional area combustor and then accelerated up to Mach 1 about 100 mm downstream of the entrance of the divergent section. A subsonic area existed around the step. The estimated combustion efficiency was 0.7 at the entrance of the divergent duct section and increased in the divergent duct section. It reached 0.9 at the exit of the downstream straight duct.

In downstream combustion ramjet mode, the estimated Mach number decreased to below unity in the divergent duct and increased to Mach 1 at the exit of the downstream straight duct without a geometrical throat. Estimated combustion efficiency increased toward the exit and reached 0.9. The choking was due to the effect of heating.

In upstream combustion ramjet mode, air flow was decelerated to a subsonic level in the vicinity of the fuel injector, and it was accelerated due to heat release by combustion within the combustor. Flow was accelerated to a supersonic level in the diverging section. In downstream combustion ramjet mode, the airflow was decelerated to subsonic level in the divergent duct, and it was accelerated up to Mach 1 at the exit of the downstream straight duct. The combustion progressed to the exit of the diverging section and the combustion gas was choked at the exit of the constant cross-sectional area combustor. The combustion efficiency increased toward the exit of the constant cross-sectional area combustor. The choking was due to the effect of heating.

C. Properties at the Exit Plane

Figures 5a–5c, 6a–6c, and 7a–7c show the distributions of the equivalence ratio, combustion efficiency, and Mach number, respectively, at the exit of the downstream straight duct. These were calculated based on gas sampling and pitot pressure data.

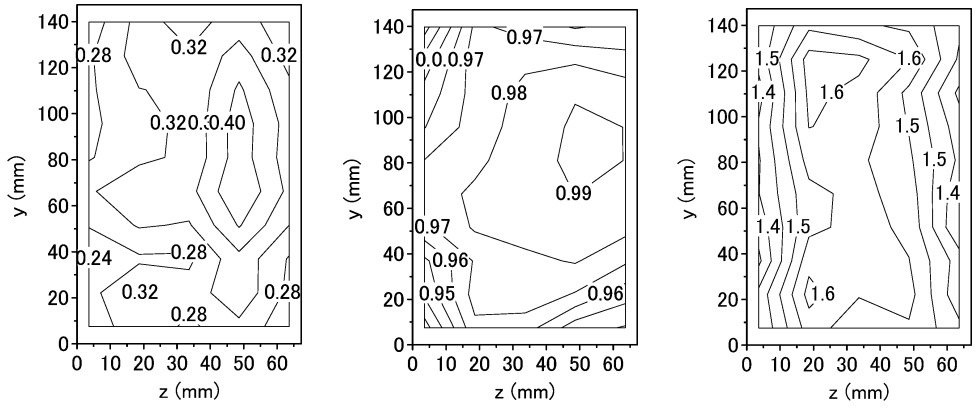

a) Equivalence ratio b) Combustion efficiency c) Mach number

Fig. 5 Distributions of equivalence ratio, combustion efficiency, and Mach number at the exit of the combustor in upstream combustion ramjet mode with equivalence ratio = 0.3.

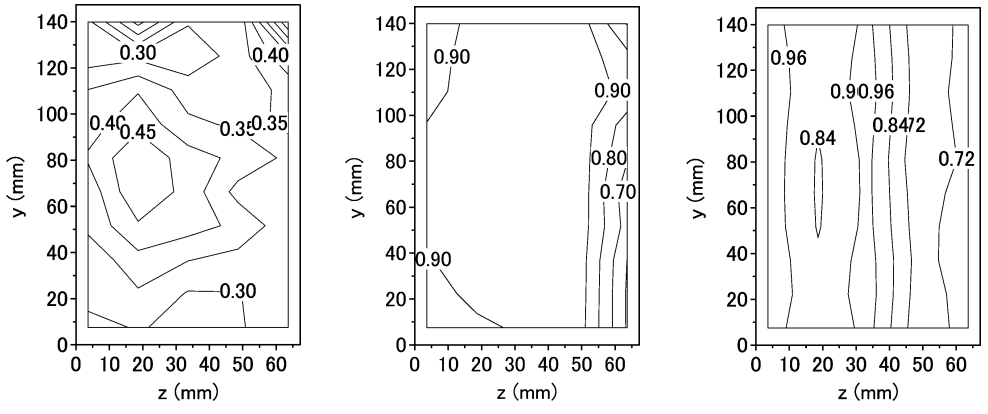

a) Equivalence ratio b) Combustion efficiency c) Mach number

Fig. 6 Distributions of equivalence ratio, combustion efficiency, and Mach number at the exit of the combustor in downstream combustion ramjet mode with equivalence ratio = 0.3.

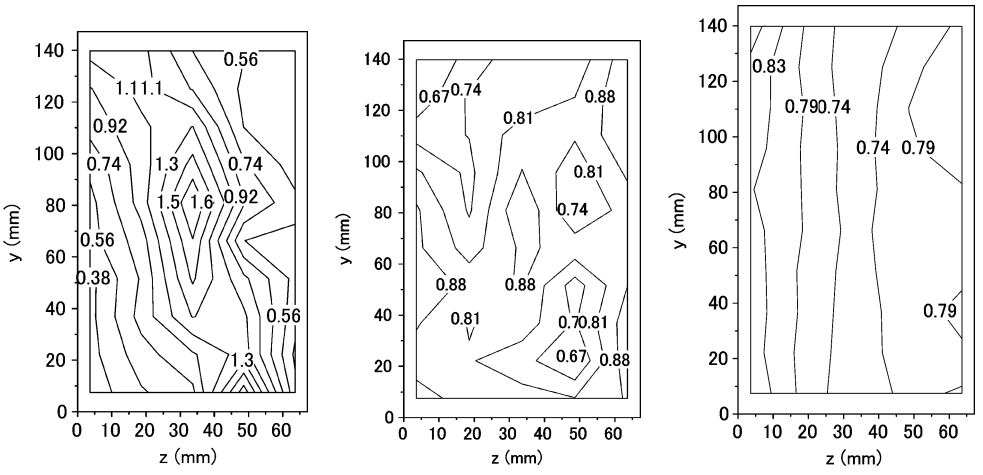

a) Equivalence ratio **b) Combustion efficiency** **c) Mach number**

Fig. 7 Distributions of equivalence ratio, combustion efficiency, and Mach number at the exit of the combustor in downstream combustion ramjet mode with equivalence ratio = 0.8.

In the case of the upstream combustion ramjet mode, the local equivalence ratio was about 0.3, which is the overall equivalence ratio, throughout the cross section, and the local combustion efficiency was around 0.98. The local Mach number was about 1.5 throughout the cross section. Though the high equivalence ratio and the combustion efficiency were distributed partially on the sidewall with five holes, the Mach number was not influenced. The average combustion efficiency at the cross section was 0.97. This was almost equal to the result of the one-dimensional analysis. This means that a good combustion condition was attained in the combustor. The averaged Mach number at the cross section was 1.50. This was almost equal to the result of the one-dimensional analysis. The impulse function calculated with the pitot pressure measurement and the gas sampling at the cross section was 3.30 kN.

In the case of the downstream combustion ramjet mode with equivalence ratio 0.3, the local combustion efficiency was around 0.9 throughout the cross section. This was smaller than that of the upstream combustion ramjet mode. The local Mach number was subsonic throughout the cross section. The average combustion efficiency at the cross section was 0.88. This was almost equal to the result of the one-dimensional analysis. The averaged Mach number on the cross section was 0.88, smaller than unity. This would be due to an error in the measurement of static pressure. The impulse function calculated based on the state of the cross section was 3.18 kN. The impulse function of the downstream combustion ramjet mode was about 4% smaller than that of the upstream combustion ramjet mode. The combustion condition was better in the case of the upstream combustion ramjet mode.

In the case of the downstream combustion ramjet mode with equivalence ratio 0.8, the local equivalence ratio was very high, especially at the center of the cross section, and the local combustion efficiency was around 0.8 throughout the cross section. This was smaller in comparison with the combustion efficiency of the downstream combustion ramjet mode with equivalence ratio 0.3. The local Mach number was subsonic throughout the cross section. The average combustion efficiency at the cross section was 0.72. The averaged Mach number at the cross section was 0.79. This was slightly smaller than unity. This would be due to an error in the measurement of static pressure. The impulse function calculated based on the state of the cross section was 3.81 kN. A higher impulse function was achieved due to a larger amount of fuel.

Figures 8a and 8b illustrate the correlations between local equivalence ratio and local combustion efficiency in the upstream combustion ramjet mode and the downstream combustion ramjet mode. In the figures, data with $\phi = 0.3$ were plotted with solid triangles and data with $\phi = 0.8$ were plotted with open squares. In the upstream combustion ramjet mode, the data with $\phi = 0.8$ were not obtained because of combustor inlet interaction.

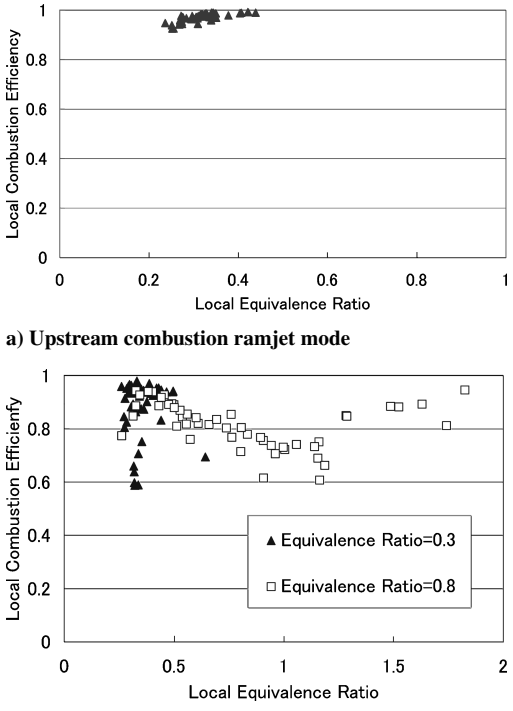

a) Upstream combustion ramjet mode

b) Downstream combustion ramjet mode

Fig. 8 Correlation between local equivalence ratio and local combustion efficiency.

In upstream combustion ramjet mode with $\phi = 0.3$, the local equivalence ratio was distributed around $\phi = 0.3$ and the local combustion efficiency has a higher value. This means that good combustion was attained.

In the case of the downstream combustion ramjet mode with $\phi = 0.3$, the local combustion efficiency has a higher value except of a few data points around $\eta_c = 0.6$. They were due to the low combustion efficiency around $z = 60$ mm in Figure 6b. This means that the combustion conditions were not uniform throughout the cross section.

In the case of the downstream combustion ramjet mode with $\phi = 0.8$, the local combustion efficiency has a lower value around the local equivalence ratio of unity. The excess H_2, when $\phi > 1$, and excess O_2, when $\phi < 1$, were sampled during the gas-sampling time. They were eventually mixed with each other in a sampling bottle, which led to lower local combustion efficiency.[12] This result means that the downstream combustion ramjet mode with $\phi = 0.8$ is primarily controlled by fuel mixing.

D. Thrust Performance

Table 1 lists the thrust performances of both upstream and downstream combustion ramjet modes at two equivalence ratios. In upstream combustion ramjet mode, a high wall-pressure distribution appeared in the straight duct part. In downstream ramjet mode, a high wall-pressure distribution appeared in the divergent duct part. A high-pressure distribution in the divergent duct would be effective for thrust generation.

The thrust calculated based on integration of the measured wall pressure was 1.14 kN in upstream combustion ramjet mode and 0.78 kN in downstream combustion ramjet mode. The friction force was estimated to be 0.17 kN in upstream combustion ramjet mode and 0.02 kN in downstream combustion ramjet mode. In the calculation of the friction force, skin-friction coefficients were calculated using White's formula.[13] In the region of pseudo-shock, flow is separated from the wall or the boundary layer becomes thick, and there is little friction force on the wall surface.[11] The friction force on the wall surface was estimated to be zero in the region of rising wall pressure. The thrust performances calculated based on wall pressure and friction were 0.97 kN in upstream combustion ramjet mode and 0.76 kN in downstream combustion ramjet mode.

The impulse function of the inlet flow was 2.62 kN according to the pitot pressure at the entrance of the isolator. The thrust performances calculated from the impulse function were 0.68 kN in upstream combustion ramjet mode and 0.56 kN in downstream ramjet mode, almost the same trend as in the case of thrust performances calculated by integration of the measured wall pressure.

The thrust performance of the upstream combustion ramjet mode was better than that of the downstream combustion ramjet mode. However, in the case of downstream combustion ramjet mode, a larger amount of fuel was available for injection. The thrusts at $\phi = 0.8$ in downstream combustion ramjet mode were 1.35 kN by wall-pressure integration and 1.19 kN by impulse function.

Table 1 shows these results.

E. Effect of Downstream Straight Duct

In the present test series, a short straight duct part with length 120 mm was attached downstream of the divergent duct part. Figure 9 shows the wall-pressure distributions of downstream combustion ramjet mode, in which squares denote the condition where there was no downstream straight duct. The equivalence ratios were 0.3 for all cases. In the case of downstream combustion ramjet mode without a downstream straight duct, the maximum wall pressure was smaller than that of downstream combustion ramjet mode with a downstream straight duct. The maximum wall pressure appeared near the fuel injection position and decreased toward the exit of the divergent duct as in the combustor with a downstream straight duct. However, the pressure at the exit was higher than the atmospheric pressure.

Table 1 Thrust performances for each case

Conditions	Impulse function [kN]	Wall pressure integration [kN]
Upstream combustion ramjet mode ($\phi = 0.3$)	0.68	0.97
Downstream combustion ramjet mode ($\phi = 0.3$)	0.56	0.76
Downstream combustion ramjet mode ($\phi = 0.8$)	1.19	1.35
Downstream combustion ramjet mode without downstream duct ($\phi = 0.3$)	0.22	0.48

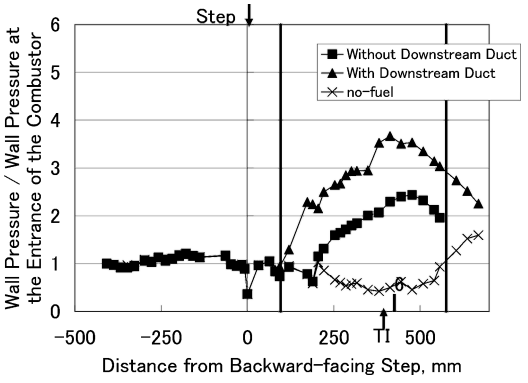

Fig. 9 Wall-pressure distributions for upstream combustion ramjet mode and downstream combustion ramjet mode and for no-straight-duct condition with downstream combustion ramjet mode with $\phi = 0.3$.

Figure 10 shows the distributions of the combustion efficiency and the averaged Mach number in downstream combustion ramjet mode without a downstream straight duct, estimated with one-dimensional calculation. The estimated averaged Mach number decreased below unity in the divergent duct and accelerated up to Mach 1 at the exit of the combustor. Subsonic combustion was attained in the divergent duct without the downstream straight duct. However, the subsonic region was narrow in comparison with that of the downstream combustion ramjet mode with a downstream straight duct.

The thrust performances in downstream combustion ramjet mode without a duct were calculated. The thrust calculated by integration of the measured wall pressure considering the estimated friction force was 0.48 kN. This was almost 40% lower than that of downstream combustion ramjet mode with a downstream straight duct. The thrust performance calculated based on the impulse function was 0.22 kN, almost 60% lower than that of downstream combustion ramjet mode with a duct. The averaged combustion efficiency at the cross section calculated based on the result of gas sampling was 0.62. This means that the downstream short straight duct is effective for greatly increasing the performance of the downstream combustion ramjet mode.

Figure 11 illustrates the correlations between the local equivalence ratio and the local combustion efficiency in downstream combustion ramjet mode without a downstream straight duct. The local combustion efficiency was widely scattered between $\eta_c = 0.0$

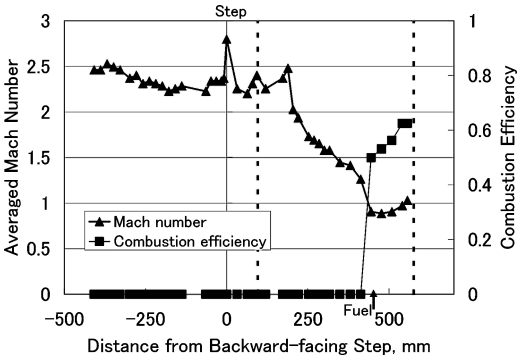

Fig. 10 Distributions of Mach number and combustion efficiency in downstream combustion ramjet mode without straight-duct.

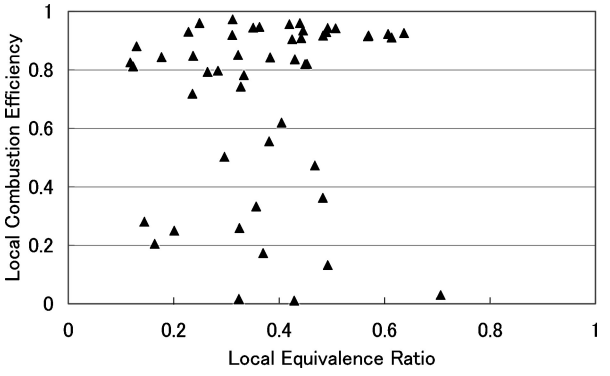

Fig. 11 Correlations between local equivalence ratio and combustion efficiency in downstream combustion ramjet mode without straight duct.

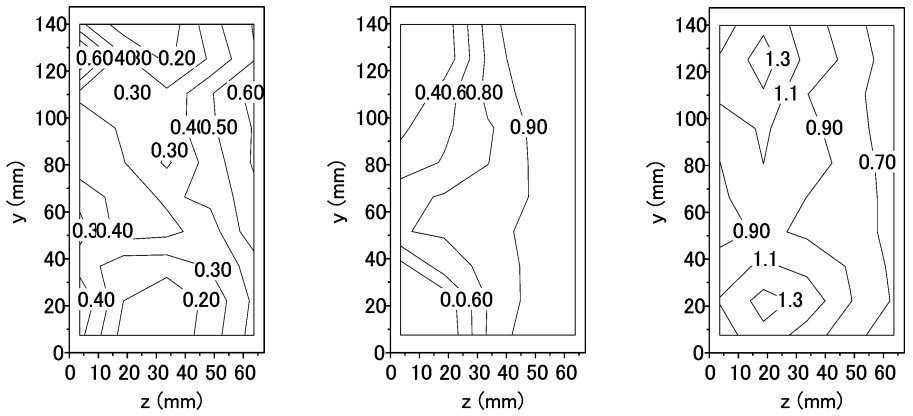

a) Equivalence ratio b) Combustion efficiency c) Mach number

Fig. 12 Distributions of equivalence ratio, combustion efficiency, and Mach number at the exit of the combustor in the downstream combustion ramjet mode without straight duct (equivalence ratio = 0.3).

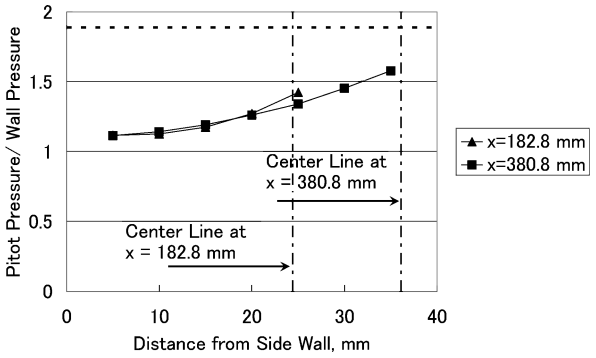

Fig. 13 Spanwise distributions of pitot pressure.

and $\eta_c = 1.0$. This denoted typical reaction-controlled combustion caused by competition between reaction speed and flow velocity.[12] These results mean that the combustion in this case is primarily controlled by the reaction. The downstream straight duct is needed for the reaction.

Figures 12a–12c show the distributions of the equivalence ratio, combustion efficiency, and Mach number, respectively, at the exit of the divergent duct. Combustion efficiency was lower than that of the downstream combustion ramjet mode with a downstream straight duct. Also, a subsonic region and a supersonic region existed at the cross section.

F. Velocity Distribution and Fuel Spread in Pseudo-Shock

To examine the conditions of the flowfield, a pitot rake was inserted into the divergent duct part. Figure 13 shows the results of the measurement of the pitot pressures at $x = 182.8$ mm and $x = 380.8$ mm. The measurement positions are shown in Fig. 2 as "P." The location of $z = 0$ mm shows that the sidewall surface has four fuel injection holes. The pitch between the pitot probes was 5 mm from the sidewall surface of $z = 0$ mm. The centerlines at each measuring position are also shown in this figure. The locations of the centerlines from the sidewall surface were $z = 24.4$ mm for $x = 182.8$ mm and $z = 36.1$ mm for $x = 380.8$ mm. The wall pressure near the probe tip was assumed to be identical to the static pressure. Measured pitot pressure P_p was normalized by this static pressure.

To investigate the velocity distribution in the cross section, the boundary between supersonic and subsonic region was estimated. We assumed that the ratio of the specific heat was almost 1.4 because the mole fraction of H_2O was not so high. Therefore, $P_p/P_s = 1.89$ was the boundary between the supersonic and subsonic regions. As a result of measurement, the flow field of the pseudo-shock in the divergent duct was expected to be in the subsonic region in the height of the centerline of the sidewall.

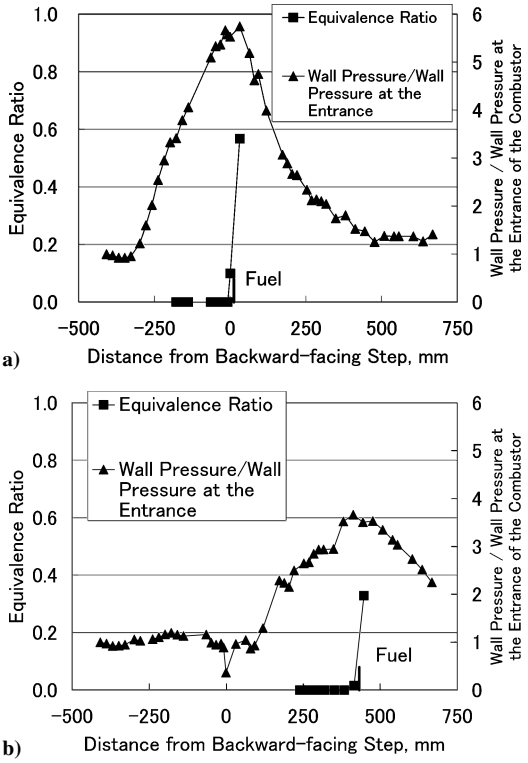

Fig. 14 Distribution of equivalence ratio with a) upstream and b) downstream fuel injection.

To investigate how far the injected fuel traveled upstream from the fuel injection position, gas sampling from the wall pressure measurement taps was conducted. Figures 14a and 14b show the distribution of the equivalence ratios resulting from the gas sampling from wall-pressure measurement taps near the fuel injection position. The distribution of wall pressure is also plotted. The fuel did not go far upstream from the fuel injection position. Though the rise in wall pressure began far upstream of the fuel injection positions, fuel did not travel upstream. This means that the fuel did not go far upstream in the separation region in the pseudo-shock. This agrees with the assumption in the one-dimensional calculation that fuel is distributed only downstream of the fuel injector.

V. Conclusions

Ramjet-mode operation in a dual-mode combustor was studied experimentally in the downstream combustion ramjet mode. The results are summarized as follows:

1) Averaged combustion efficiency at the exit of the downstream straight duct in downstream combustion ramjet mode was lower than that in upstream combustion ramjet mode, 0.88 and 0.97, respectively. The best thrust performance was attained in upstream combustion ramjet mode. The thrust at $\phi = 0.3$ in upstream combustion ramjet mode was 20 to 30% higher than that in downstream combustion ramjet mode. In downstream combustion ramjet mode, however, it was possible to inject a larger amount of fuel. This was available to generate larger thrust.

2) The downstream combustion ramjet mode with large equivalence ratio was primarily controlled by fuel mixing.

3) The fuel did not go upstream from the fuel injection position.

4) In downstream combustion ramjet mode, even with no downstream straight duct, subsonic combustion was also attained. However, the thrust performance was lower than that in downstream combustion ramjet mode with a downstream straight duct. This was due to insufficient residence time for mixing.

References

[1]Heiser, K. H., Pratt, D. T., Daley, D., and Mehta, U. B., "Hypersonic Airbreathing Propulsion," AIAA Education Series, AIAA, Washington, DC, 1994, pp. 334–370.

[2]Sullins, G. A., "Demonstration of Mode Transition in a Scramjet Combustor," *Journal of Propulsion and Power*, Vol. 9, No. 4, 1993, pp. 515–520.

[3]Kanda, T., Chinzei, N., Kudo, K., and Murakami, A., "Dual-Mode Operation in a Scramjet Combustor," AIAA Paper 2001-1816, 2001.

[4]Kobayashi, K., Tomioka, S., Kato, K., Murakami, A., Kudo, K., and Mitani, T., "Performance of a Dual-Mode Combustor with Multi-Staged Fuel Injection," AIAA Paper 2004-3482, 2004.

[5]Kanda, T., and Kudo, K., "Conceptual Study of a Combined-Cycle Engine for an Aerospace Plane," *Journal of Propulsion and Power*, Vol. 19, No. 5, 2003, pp. 859–867.

[6]Kobayashi, K., Tomioka, S., and Mitani, T., "Supersonic Flow Ignition by Plasma Torch and H_2/O_2 Torch," *Journal of Propulsion and Power*, Vol. 20, No. 2, 2004, pp. 294–301.

[7]Mitani, T., Takahashi, M., Tomioka, S., Hiraiwa, T., and Tani, K., "Analysis and Application of Gas Sampling to Scramjet Engine Testing," *Journal of Propulsion and Power*, Vol. 15, No. 4, 1999, pp. 572–577.

[8]Waltrup, P. J., and Cameron, J. M., "Wall Shear and Boundary-Layer Measurement in Shock Separated Flow," *AIAA Journal*, Vol. 12, No. 6, 1974, pp. 878–880.

[9]Ostras, V. N., and Penzin, V. I., "Experimental Study of Friction in a Channel with a Pseudoshock," *Fluid Mechanics—Soviet Research*, Vol. 4, No. 6, 1975, pp. 32–38.

[10]Carroll, B. F., and Dutton, J. C., "Characteristics of Multiple Shock Wave/Turbulent Boundary-Layer Interactions in Rectangular Ducts," *Journal of Propulsion and Power*, Vol. 6, No. 2, 1990, pp. 186–193.

[11]Heiser, K. H., Pratt, D. T., Daley, D., and Mehta, U. B., Hypersonic Airbreathing Propulsion, AIAA Education Series, AIAA, Washington, DC, 1994, pp. 251–256.

[12]Mitani, T., Chinzei, N., and Kanda, T., "Reaction and Mixing-Controlled Combustion in Scramjet Engines," *Journal of Propulsion and Power*, Vol. 17, No. 2, 1991, pp. 308–314.

[13]White, F. M., *Viscous Fluid Flow*, McGraw–Hill, New York, 1974, pp. 641–644.